A Numerical Study of the Take-Off Dynamics of the *TNPS, Tri-K and U* Sliders

Liangsheng Chen

David B. Bogy

Computer Mechanics Lab

University of California at Berkeley

June 1997

Contents

List of Tables

List of Figures

Abstract

In this report, the dynamic characteristics of the "pico-size" *TNPS, Tri-K* and *U-rail* sliders are first investigated and compared by use of *CML*'s dynamic simulator to study the bump and impulse responses. A modal analysis method is used to obtain the stiffness and damping ratios of these air bearings. Then the dynamic simulator was used to study the contact take off dynamics. It is found that the air bearing of the U slider is the stiffest while those of the Tri-K and the TNPS slider have much larger damping ratios than that of the U slider. During the contact take-off process, the U slider has the smallest take off velocity (TOV) and performs best as far as wear is concerned while the TNPS slider performs worst. The effects of the suspension parameters and media surface parameters are also investigated.

1 Introduction

The dynamic characteristics of a slider are important factors in air bearing design. In this report the dynamic performance of three pico sliders (30% form-factor), designated as the *TNPS*, *Tri-K*, and *U-rail* sliders are first investigated using *CML*'s Air Bearing Dynamic Simulator. The air bearings' responses to impulse excitations in the vertical, pitch and roll directions are simulated. The results are then used with the new modal analysis software (PIP) developed at CML to obtain the modal parameters, such as natural frequency, damping ratio and stiffness.

Before a slider fully takes off it remains in sliding contact with the disk surface, which inevitably causes wear damage to the head disk interface. One of the key parameters affecting the tribological performance of the head disk interface is the take-off velocity (TOV). With a higher TOV, the sliding distance between the head and disk is longer. Since the wear volume is assumed to be proportional to the sliding distance of two surface in relative motion, it is desirable for the slider to have a small TOV in order to improve the head disk interface durability. Therefore, a thorough understanding of the sliding contact process and the dependence of TOV and wear on the slider geometry and drive configuration are necessary.

Zhu and Bogy [1] found that negative crown causes more disk wear than positive crown. Suk et al. [2] used the multi-channel laser interferometer to investigate the influence of crown on slider dynamics during take-off. They concluded that sliders with positive crown may cause less wear due to their shorter sliding distance and less probability of point contacts with the disks. Suzuki and Hayashi [3] carried out an experimental study of the parameters that determine TOV and CSS performance of thin film disks. They showed that higher clamping force could drastically deteriorate the CSS durability. The reason is that the clamping force introduces short range waviness on a disk, which affects the slider's flyability. Lee et al. [4] investigated the dependence of TOV and friction on selected head parameters using an air bearing spindle equipped with a strain gauge. They showed that for the thin film head, crown had the greatest influence on TOV, followed by bolt pattern runout, suspension

preload, camber, skew angle and rail width in decreasing order. They also showed that both crown and skew angle affect the coefficient of friction between the head and disk. Bolasna [5] numerically analyzed the effects of slider/suspension parameters on the TOV of a taper flat slider and a shaped IBM 3380K slider. He found that crown is the most significant parameter affecting the TOV. However, he didn't consider the actual slider/disk contact. Hu and Bogy [6] conducted a numerical study of the contact take-off process of the nano-size Nutcracker slider. They found that the slider's crown and disk surface roughness are the most significant parameters affecting the TOV.

It is estimated that about 15% of the sliders will be pico heads by the end of 1997, with a projected increase to 50% by the end of 1998 [7]. Since pico sliders are more sensitive to forces exerted by the suspension and disk than nano sliders, we first compared the contact take off performance of three pico sliders. Then we further looked into those factors such as suspension and disk surface parameters, that might affect the contact take off performance.

2 Theoretical Models and Numerical Methods

2.1 Air Bearing Model

The pressure distribution between the slider and the rotating disk can be described by the compressible Reynolds equation. The generalized Reynolds equation can be written in the non-dimensionalized form as:

$$\frac{\partial}{\partial X}[\hat{Q}PH^3\frac{\partial P}{\partial X} - \Lambda_X PH] + \frac{\partial}{\partial Y}[\hat{Q}PH^3\frac{\partial P}{\partial Y} - \Lambda_Y PH] = \sigma\frac{\partial}{\partial T}[PH], \tag{1}$$

where, $\Lambda_X = 6\mu UL/p_a h_m^2$ and $\Lambda_Y = 6\mu VL/p_a h_m^2$ are the bearing numbers in the x and y directions, and $\sigma = 12\mu\omega L^2/p_a h_m^2$ is the squeeze number, and $\hat{Q}$ is the Poiseuille flow factor.

2.2 Slider Dynamics

The two-dimensional motion of an air bearing slider flying over a rotating disk is described by:

$$\begin{aligned} m\ddot{z} &= F + \int_A (p - p_a) dA \\ I_\theta \ddot{\theta} &= M_\theta + \int_A (p - p_a)(x_g - x) dA \\ I_\phi \ddot{\phi} &= M_\phi + \int_A (p - p_a)(y_g - y) dA, \end{aligned} \tag{2}$$

where, $z,\ \theta,\ \phi$ are the vertical displacement, pitch and roll, respectively. $I_\theta,\ I_\phi$ are moments of inertia, $x_g,\ y_g$ are the positions of the slider's center of gravity, and $F,\ M_\theta,\ M_\phi$ are the force and moments exerted on the slider by the suspension. If contact occurs, then $F,\ M_\theta,\ M_\phi$ are the resultant force and moments exerted on the slider by the suspension and disk.

2.3 Contact and Wear Models

The asperity-based elastic-plastic contact model proposed by Chang et al. [12] is used to estimate the contact force and moment. The following assumptions are made in this model:

1. the rough surface is isotropic,
2. the asperities are spherically-shaped near their summits with the same radius before contact,
3. the asperities height distribution is Gaussian,
4. there is no interaction between asperities,
5. there is no bulk deformation

The wear estimation is based on the Archard's wear equation, i.e., the amount of wear is proportional to the frictional work done. Hence if the maximum allowable wear volume is

known, then the durability of the head disk interface can be estimated as:

$$Durability = \frac{Total\ Allowable\ Wear\ Volume}{Wear\ Volume\ in\ Each\ Cycle} \tag{3}$$

2.4 Numerical Methods

The dynamic analysis of a slider flying over a rotating disk requires simultaneous solution of equations (1)-(2) and the dynamics of the suspension.

The generalized Reynolds equation (1) is discretized using Pantakar's control volume method [8][9] and solved using the alternating direction line sweeping method combined with a multi-grid method [10] [11]. The coupled equations are solved using the Newmark-β method. A modal truncation method is used to include the suspension dynamics.

3 Results and Discussion

Figure 1(a) and 1(b) show the 2-D rail shape and air bearing pressure profile for the *TNPS* slider. From Figure 1(a) we can see that the TNPS slider is asymmetric. The maximum recess depth is 3.332 μm. The rails have certain ramp wall profiles. It has a crown of 20.32 nm.

The *Tri-K* slider as shown in Figure 2(a) has a recess depth of 10.16μm and a crown of 25.4 nm. Figure 2(b) shows its air bearing pressure profile.

Figure 3(a) shows the *U-rail* slider, which has a recess depth of 3.556 μm and a crown of 20.32 nm. The *U-rail* slider's air bearing pressure profile is shown in Figure 3(b).

In the following discussion, unless otherwise specified, it is assumed that the full speed of the disk is 7200 RPM, the disk radius at which the slider flies is 20.5 mm, the skew angle is 7.524 degrees, and the suspension preload is 2.5 g. The sliders' flying altitudes at center trailing edge under these conditions are summarized in Table 1.

3.1 Impulse Responses

In order to investigate the dynamic characteristics of the three air bearings, we simulated their responses to impulsive excitations in the vertical, pitch and roll directions. Figures 4- 6 illustrate the three sliders' dynamic responses to a vertical impulse of 0.2 cm/s. Figures 7 - 12 show the sliders' dynamic response in both the time domain and frequency domain after the sliders are subjected to pitch and roll impulses of magnitude 4 rad/s, respectively. These results were used to obtain the modal parameters of the air bearings as discussed in the following section.

3.2 Air Bearing Stiffness and Damping

In addition to nominal flying height uniformity, two characteristics that are desired in a slider air bearing are high air-bearing stiffness and high damping. Air-bearing stiffness gives a measure of the stability and control that can be expected from the HDI when the slider is subjected to dynamic input. High stiffness also is usually a measure of how sensitive the static flying height will be to the various manufacturing tolerances involved.

The damping of a slider is due to the viscous dissipation of energy on the slider air-bearing surface. As flying height decreases, generally the air bearing loses some of its damping capability. The air bearing at the HDI of a hard disk drive is already highly under-damped, so the air bearing damping is a property of increasing interest as flying heights continue to decrease toward zero. At flying heights that produce intermittent contacts with a rough disk surface, it is very important to understand and control both the stiffness and the damping characteristics of new slider designs.

Using a modal analysis software developed at CML [13], we calculated the air bearing stiffness and damping ratios from the sliders' impulse responses. Table 2 lists the air bearing stiffnesses for the three pico sliders. From Table 2 we can see that the U slider air bearing is the stiffest, whereas the Tri-K slider air bearing is the least stiff. For the Tri-K slider, the outer rails do not extend to the lowest clearances and thus do not produce significant

roll stiffness, which leads to larger roll angle and roll angle variation. The lack of full-length outer rails also cause the resulting air-bearing to have less vertical stiffness. The trailing pad of the Tri-K slider generates air bearing load only through pitch and roll orientation (the wedge effect) to the disk and thus suffers from relatively low local air bearing stiffness.

Tables 3 and 4 list the natural frequencies and damping ratios for the three designs. In both tables, mode 1 is mainly in pitch motion (rear end) for all the sliders, while mode 2 of the TNPS slider and mode 3 of the Tri-K and U sliders are mainly in roll motion. From Table 4 we can see that the U slider exhibits the smallest damping, which is attributed to the rail geometry since there are few "outlets" to dissipate energy. On the contrary, the rail shapes of the Tri-K and TNPS sliders lead to much higher damping.

3.3 Bump Responses

In order to verify the stiffness and damping data shown in Tables 2 and 4, and to eventually compare the simulation with experimental results, we numerically investigated the sliders' responses to the passage of a 10 nm high rectangular bump.

Figures 13, 14 and 15 show the track profile, and the modulations of flying height, pitch and roll of the TNPS, Tri-K and U sliders due to the disk bump. These results substantiate the stiffness and damping data previously obtained.

3.4 Contact Start-Up Dynamics

From the above results we can see that the three sliders are quite different as far as the dynamic performance is concerned. The question now is how do they perform differently in the CSS process and what are the determining factors that affect their CSS performance.

3.4.1 Effect of Disk Spin-up Time

In real disk drive operation, it usually takes about 3 seconds for the disk to spin up to 3000 RPM. Obviously, it's impractical to do dynamic simulation with this kind of ramp-up profile

because of the small time step required. On the other hand, a "numerically- accelerated" spin-up profile might introduce artificial dynamic effects. In order to find an appropriate disk spin-up time for the numerical takeoff study, we did simulations using the TNPS slider with spin-up times of 2 ms, 10 ms and 20 ms for the disk to accelerate to 2000 RPM. Figure 16 clearly shows that some artificial dynamic effects could be introduced with an assumed spin-up time that is too short. In the figure, the "quasi-static" data were obtained with a series of constant disk speed simulations. From Figure 16 we can see that a spin-up time of 20ms (up to 2000 RPM) is appropriate for our study, since the results for this acceleration are very close to the "quasi-static" case.

3.4.2 Comparison of the Three Designs

Figures 17 - 19 show the contact force, trailing edge nominal flying height, pitch and roll vs. disk speed for the TNPS, Tri-K and U sliders.

For comparison, we plot the contact force, friction work and friction power vs. disk speed for the three designs together in Figure 20. From Figure 20 we can see that the U slider performs the best due to the smallest TOV, contact force and hence least friction work as demonstrated in Figure 20(b). In the calculation of friction work, a constant value of 0.3 for the dynamic coefficient of friction was assumed, although Lee et al. [4] showed that both crown and skew angle affect the coefficient of friction. The fact that the TNPS slider performs even worse than the Tri-K slider is somewhat contrary to our expectation since the general belief is that a stiffer air bearing usually takes off faster.

3.4.3 Crown Effect

Figure 21 demonstrates the effect of the slider's crown on the TOV and contact force for the TNPS slider. The two crown values used for comparison were 10 nm and 20 nm. We can see that in a certain range, a larger value of crown will lead to a smaller TOV, contact force and hence less wear.

3.4.4 Suspension Effect

We also did a comparative study on the TNPS slider with two types of suspensions, namely, the 830 NF2 and FX30U. The suspension preloads were both 2.5 g. From Figure 22, we can see that the suspension dynamics indeed has almost no effect on either the contact force or the flying characteristics in the contact take off process.

However from Figure 23, we can see that a smaller suspension preload leads to faster take off and obviously a smaller contact force. The simulation was done on the TNPS slider with 2.5g and 1.5 g preloads, respectively.

3.4.5 Effect of Media Surface Parameters

As stated in section 2.3, we assume a Gaussian distribution of the asperity heights. An important parameter of this model is the standard deviation of the height distribution. In certain cases, it may correlate with the RMS value of disk roughness. To investigate its effect, we did simulations with standard deviation values of 3 nm and 6 nm. From Figure 24 we can see that a smaller value of standard deviation, i.e. a smoother disk surface, leads to a smaller TOV and thus less wear.

As shown in Figure 25 we also compared the effects of disk asperity density. It appears that even when we double the density of asperities, the changes in contact force and TOV are small.

In our model, the dynamic friction force was included as follows:

$$f = \mu N \tag{4}$$

where, μ is the dynamic friction coefficient and N is the contact force. In the previous results, μ was chosen to have the constant value of 0.3. From Figure26 we can see that an increase of μ from 0.3 to 0.6 has some effect on the flying attitude of the slider since a larger friction force will decrease the pitch angle and thus increase the center trailing flying height. The influence on the contact force and TOV is minor. However, wear will increase since the friction increases.

4 Conclusion

The dynamic characteristics of the TNPS, Tri-K and U sliders were investigated using CML's dynamic simulator. The U slider air bearing is found to be the stiffest one while the Tri-K slider air bearing is the least stiff. The numerical simulation results for the sliders' bump responses and impulse responses clearly illustrate their dynamic characteristics. The U slider has the smallest TOV and is expected to cause the least wear, whereas the TNPS slider has the largest TOV and causes the most wear among the three designs studied here. A smaller crown will lead to a smaller TOV and contact force and hence less wear. The suspension dynamics has little effect on the contact take-off process whereas a smaller suspension preload leads to faster take off and less wear. The standard deviation of the asperity height distribution affects the contact take off process significantly while the asperity density seems to have less effect.

5 Acknowledgment

This work is supported by the Computer Mechanics Laboratory at the University of California at Berkeley and Quantum Corp. We would like to thank Geoff Kaiser and Pete Griffin of Quantum Corp. for providing the slider design data and valuable discussions.

References

[1] Zhu,L.Y. and Bogy, D.B., 1989, "A Multi-channel Laser Interferometer and Its Use to Study Head-Disk Interface Dynamics in Magnetic Disk Drive," *Tribology and Mechanics of Magnetic Storage Systems*, STLE Special Publication, **VI**, pp.168-179.

[2] Suk, M., Ishii, T. and Bogy, D.B., 1992, "The Influence of Air-Bearing Surface Geometry on the Dynamics of Sliders," *ASME Journal of Tribology*, **114**, pp.26-31.

[3] Suzuki, S., Hayashi, I. and Matsushita, K., 1993, "An Experimental Study of the Parameters that Determine Take-Off Velocity and CSS Performance of Thin Film Disks," *Tribology Transactions*, bf 36(3), pp.411-416.

[4] Lee, J.K., Enguero, J., Smallen, M., Chao, A. and Cha, E. , 1995, "The Dependency of Takeoff Velocity and Friction on Head Geometry and Drive Configuration," *ASME Journal of Tribology*, **117**, pp.350-357.

[5] Bolasna, S., 1990, "Air Bearing Parameters Effects on Take-off Velocity," *IEEE Transaction on Magnetics*, **26**(6), pp.3033-3038.

[6] Hu, Y. and Bogy, D.B., 1995, "Numerical Study of A Slider's Contact Take-off Process", *Technical Report No. 95-009*, Computer Mechanics Laboratory, U.C. Berkeley.

[7] Carlson, P., "Advancing Suspension Performance for the 30% Form Factor," *IDEMA Insight*, May/June, 1997, pp.4.

[8] Pantakar, S.V., 1980, *Numerical Heat Transfer and Fluid Flow*, McGraw-Hill.

[9] Cha, E. and Bogy, D.B., 1995, "A Numerical Scheme for Static and Dynamic Simulation of Sub-ambient Pressure Shaped Rail Sliders," *ASME Journal of Tribology*, **117**, pp.36-46.

[10] Hutchinson, B.R. and Raithby, G.D., 1986, "A Multigrid Method Based on the Additive Correction Strategy," *Numerical Heat Transfer*, **9**, pp.511-537.

[11] Lu, S. and Bogy, D.B., "A Multi-Grid Control Volume Method for the Simulation of Arbitrarily Shaped Slider Air Bearing with Multiple Recess Levels," *CML Technical Report*, **94-016**.

[12] Chang, W.R., Etsion, I. and Bogy, D.B., 1987, "An Elastic-Plastic Model for the Contact of Rough Surfaces," *ASME Journal of Tribology*, **109**, pp.257-263

[13] Zheng,Q.-H., Chen,L. and Bogy, D.B., "A Modal Analysis Method for Slider Air Bearings in Hard Disk Drives," *CML Technical Report*, **96-021**.

Slider	Flying Height (nm)	Pitch (μrad)	Roll (μrad)
TNPS	43.31	159.20	-5.71
Tri-K	39.26	212.92	13.01
U	45.03	141.38	-10.07

Table 1: Flying altitudes for TNPS, Tri-K and U sliders

Slider	Vertical (kN/m)	Pitch (mN-m/rad)	Roll(mN-m/rad)
TNPS	843.5	137.7	101.2
Tri-K	533.4	65.1	69.8
U	1020.0	163.7	152.7

Table 2: Comparison of air bearing stiffness

Slider	Mode 1 (kHz)	Mode 2 (kHz)	Mode 3 (kHz)
TNPS	89.2	131.7	145.9
Tri-K	63.4	106.8	112.4
U	102.3	155.5	163.8

Table 3: Comparison of air bearing natural frequency

Slider	Mode 1	Mode 2	Mode 3
TNPS	4.08	2.28	2.18
Tri-K	4.66	2.20	2.21
U	1.38	0.95	1.03

Table 4: Comparison of air bearing damping

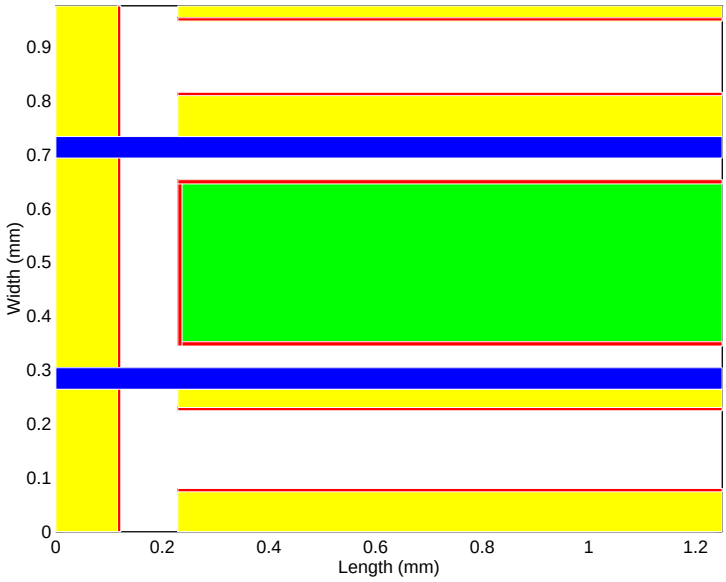

(a) Rail shape

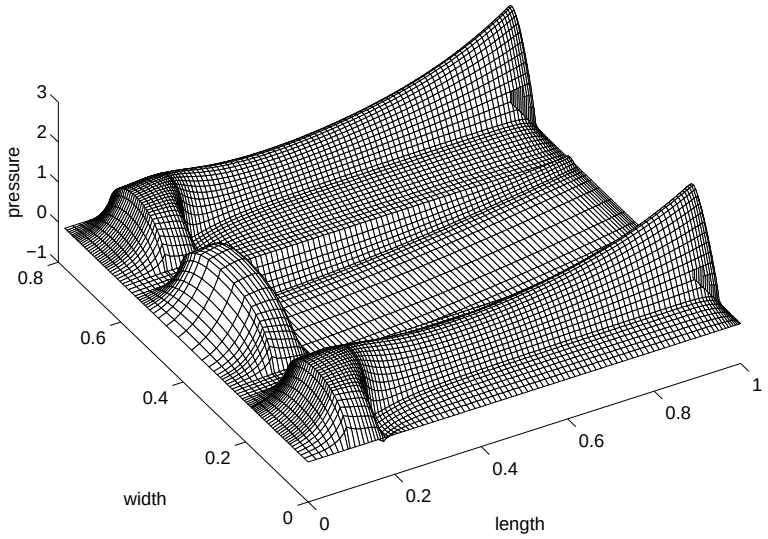

(b) Pressure Profile

Figure 1: Rail shape and pressure profile for 30% TNPS slider

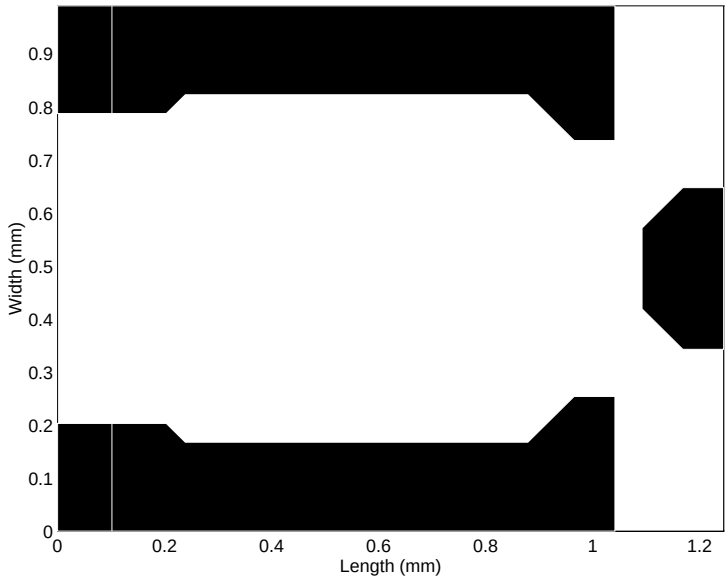

(a) Rail shape

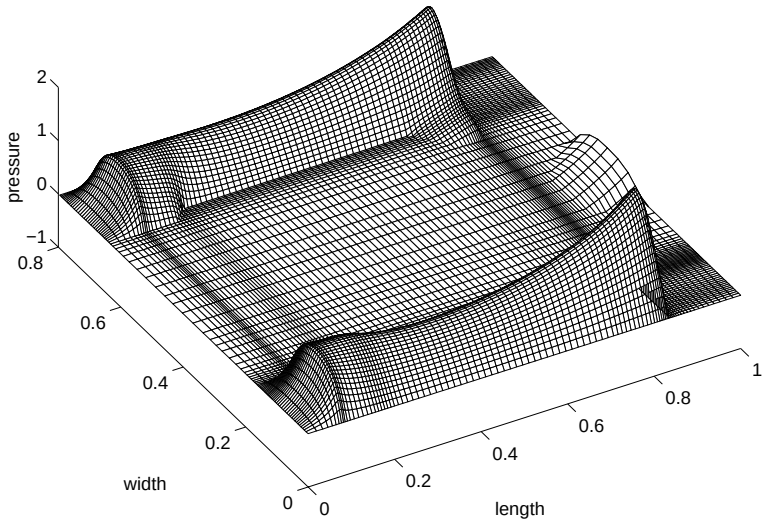

(b) Pressure profile

Figure 2: Rail shape and pressure profile for 30% Tri-K slider

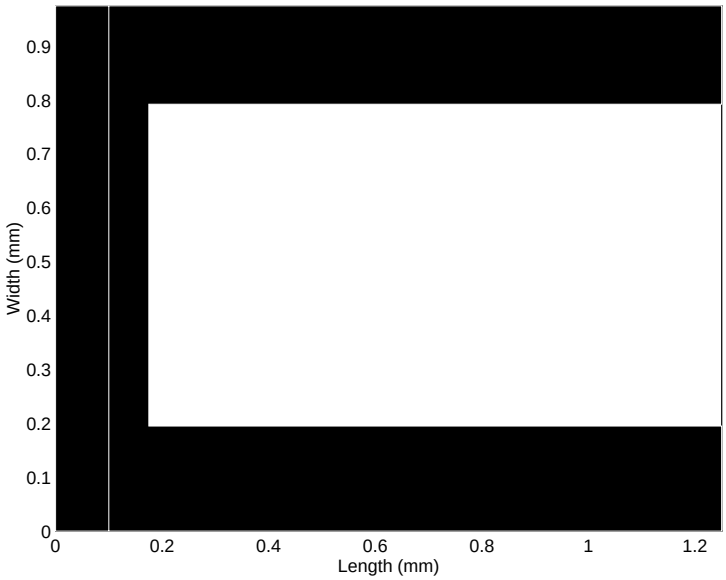

(a) Rail shape

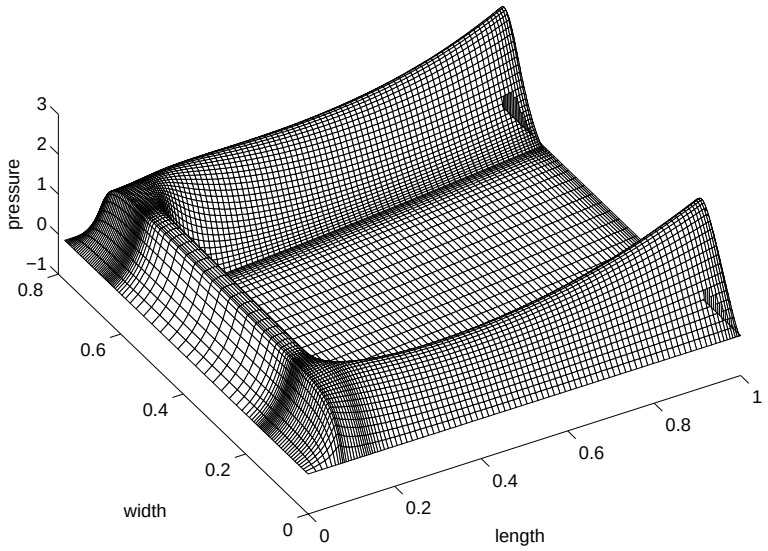

(b) Pressure Profile

Figure 3: Rail shape and pressure profile for 30% U slider

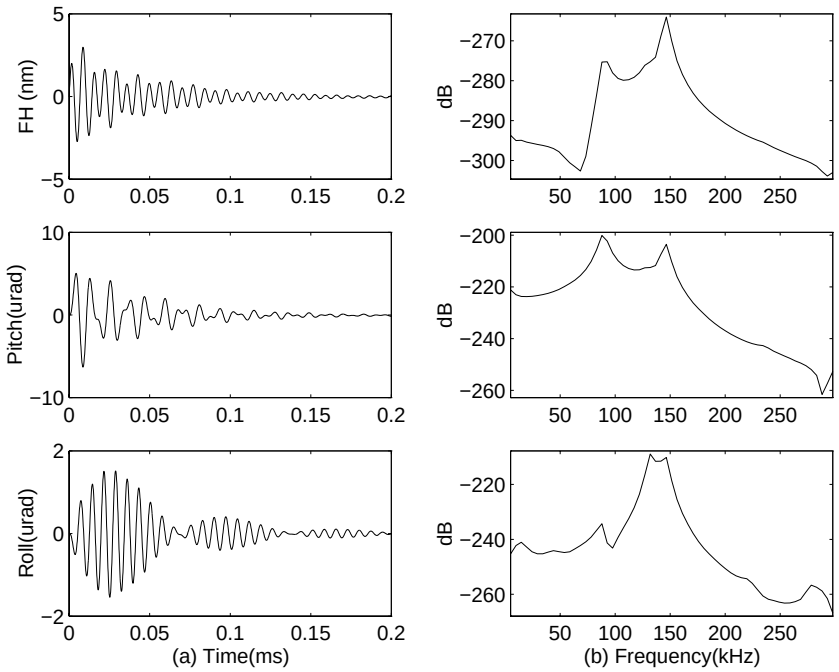

Figure 4: Responses of the 30% TNPS slider to a vertical impulse of 0.2cm/s

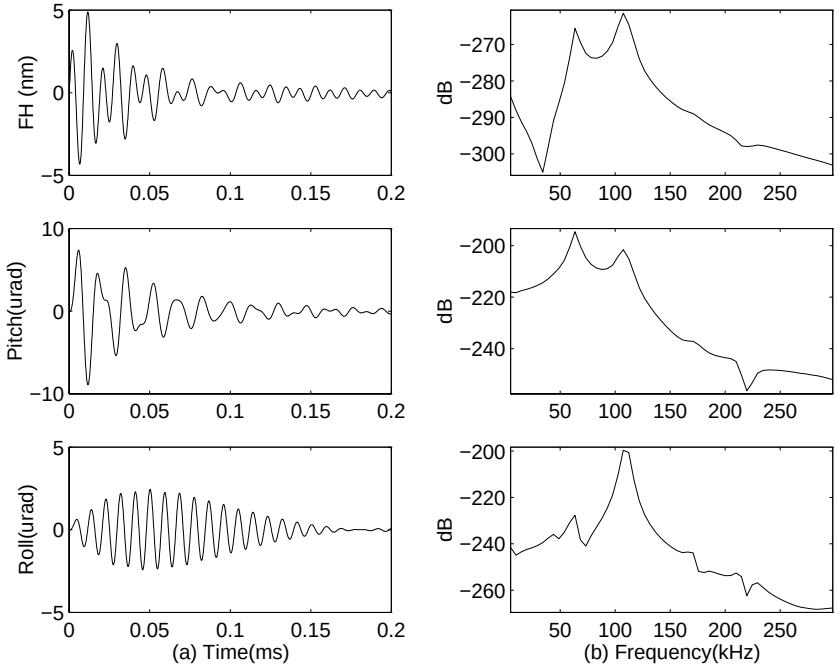

Figure 5: Responses of the 30% Tri-K slider to a vertical impulse of 0.2cm/s

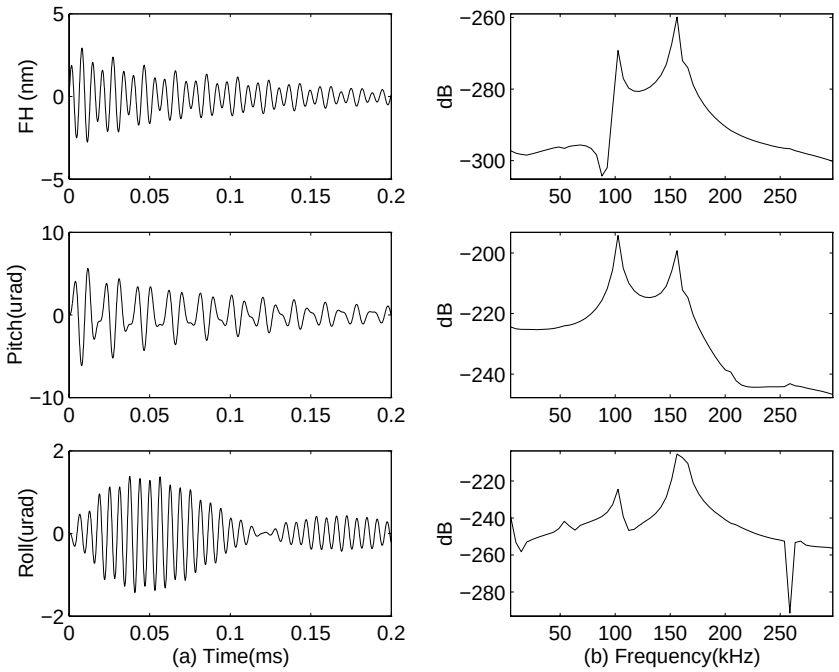

Figure 6: Responses of the 30% U slider to a vertical impulse of 0.2cm/s

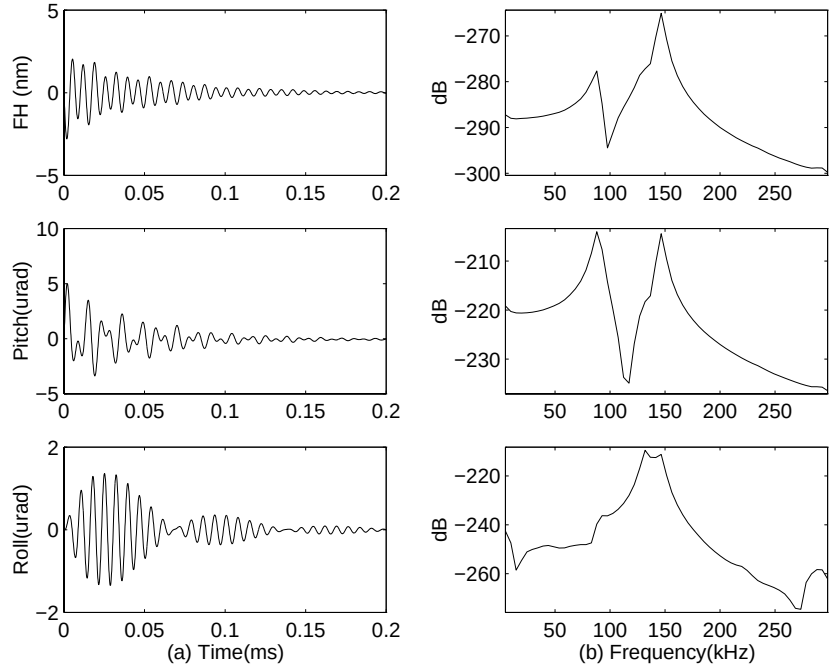

Figure 7: Responses of the 30% TNPS slider to a pitch impulse of 4 rad/s

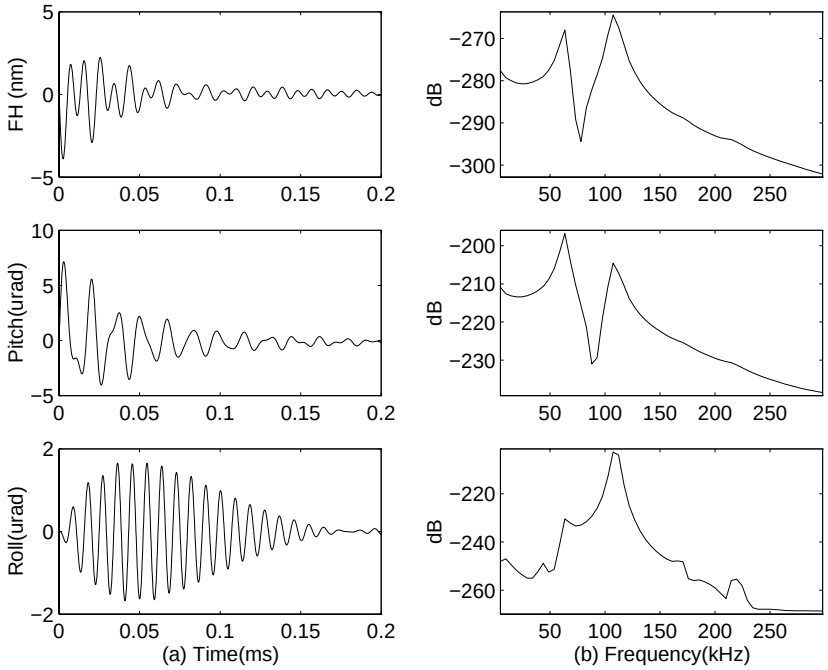

Figure 8: Responses of the 30% Tri-K slider to a pitch impulse of 4 rad/s

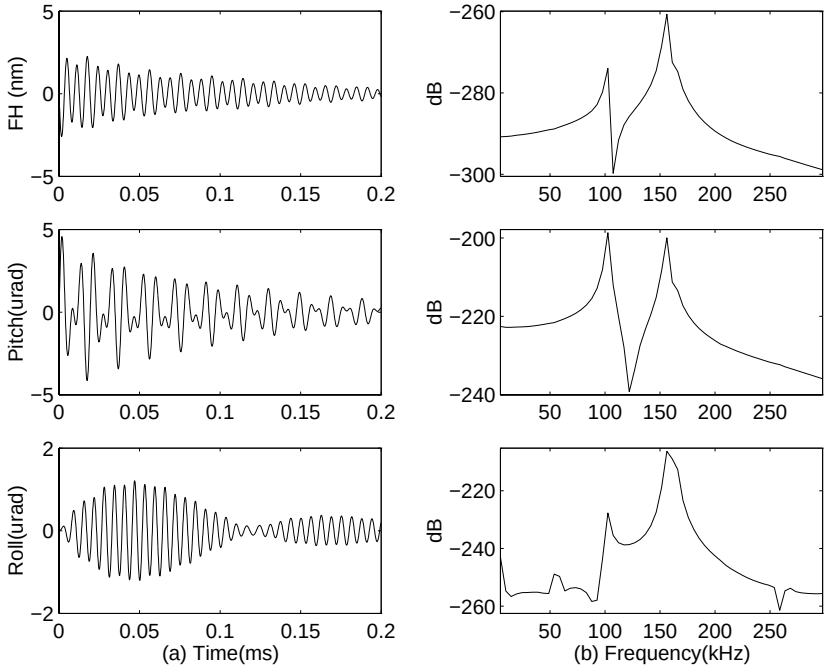

Figure 9: Responses of the 30% U slider to a pitch impulse of 4 rad/s

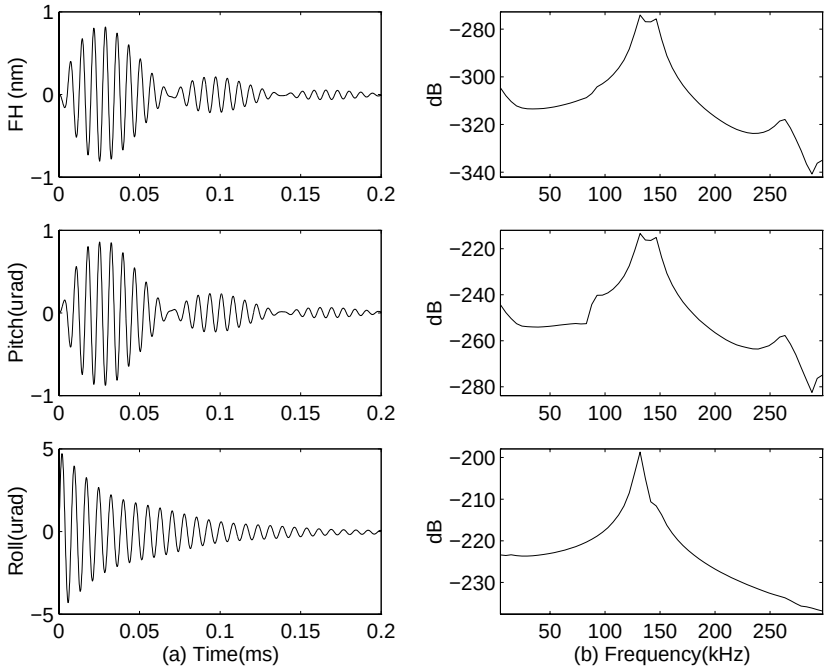

Figure 10: Responses of the 30% TNPS slider to a roll impulse of 4 rad/s

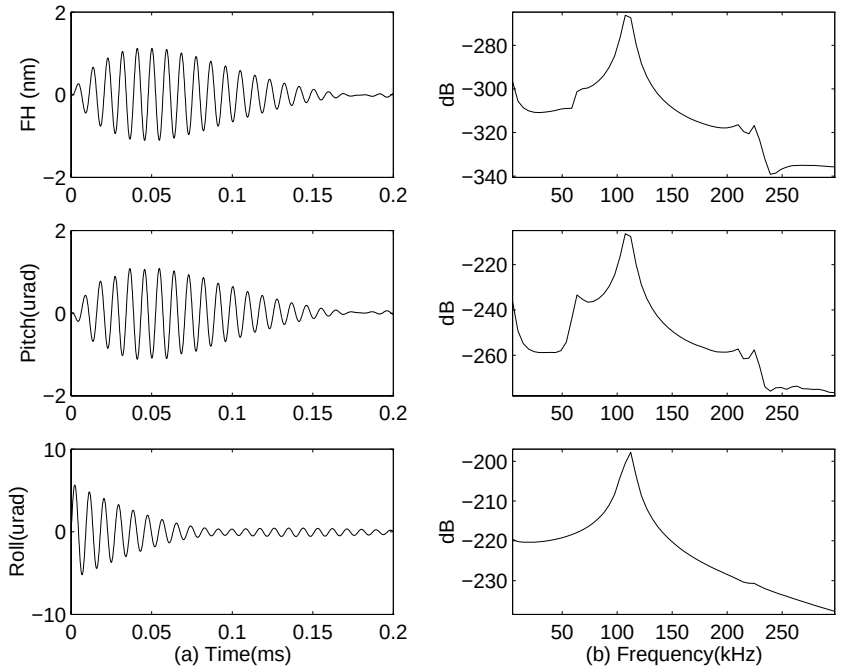

Figure 11: Responses of the 30% Tri-K slider to a roll impulse of 4 rad/s

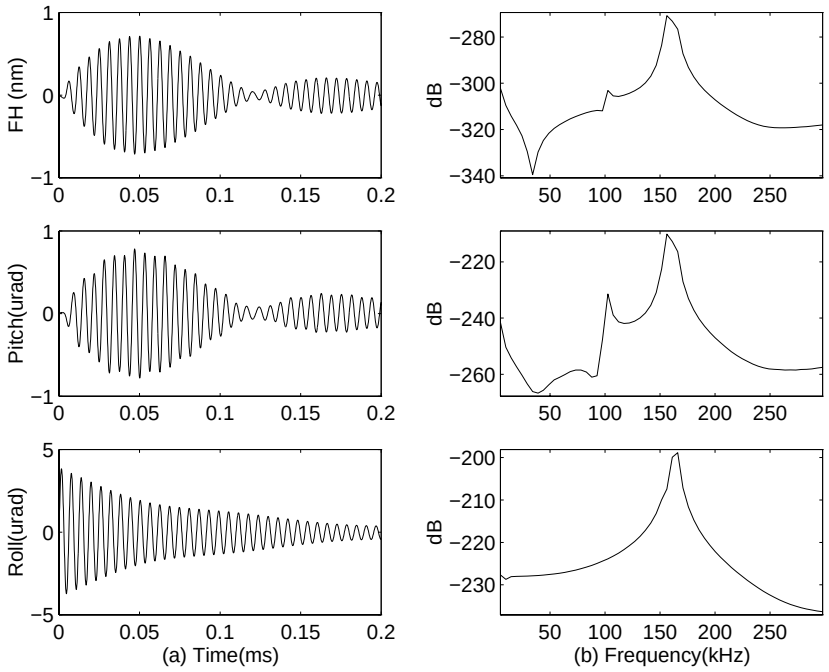

Figure 12: Responses of the 30% U slider to a roll impulse of 4 rad/s

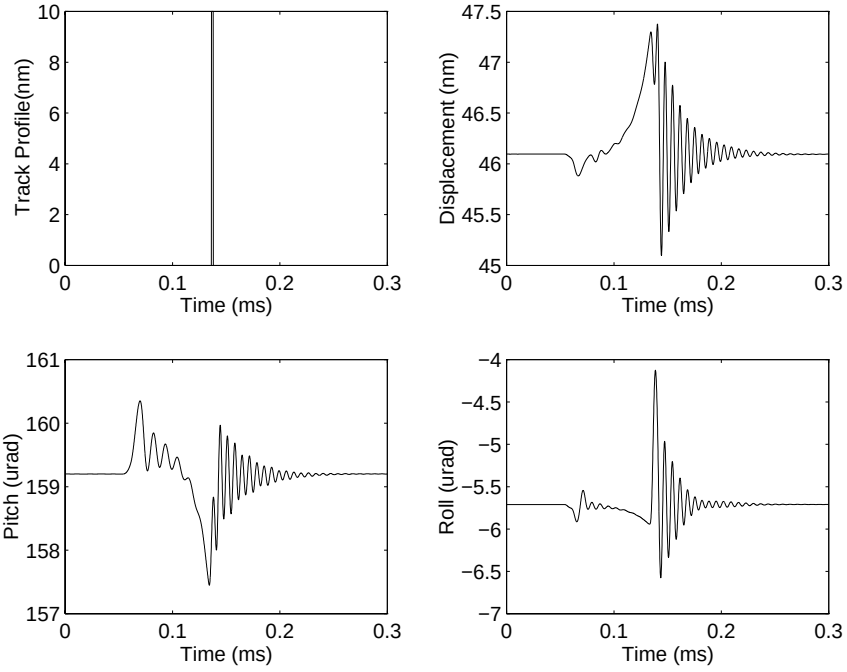

Figure 13: Responses of the 30% TNPS slider to a 10 nm bump

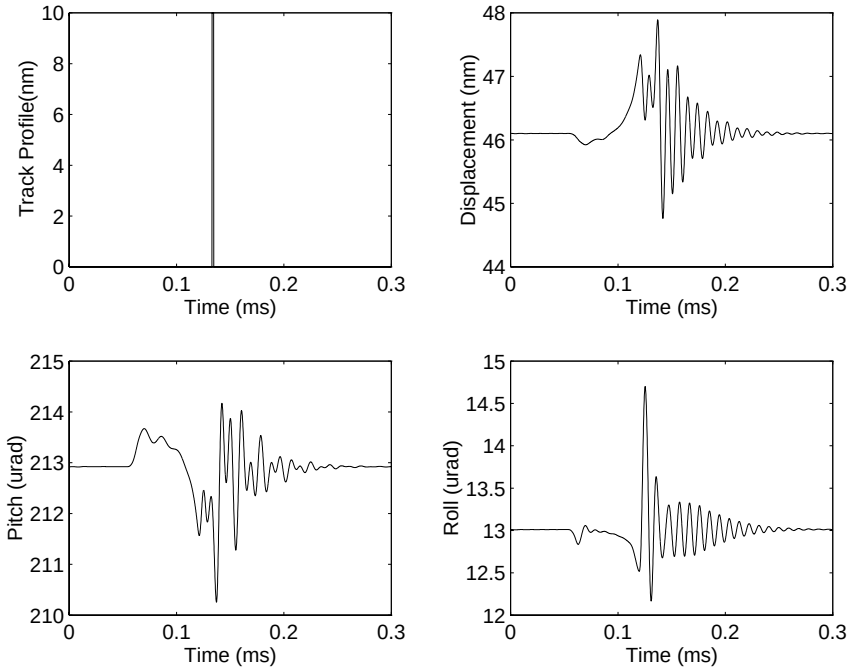

Figure 14: Responses of the 30% Tri-K slider to a 10 nm bump

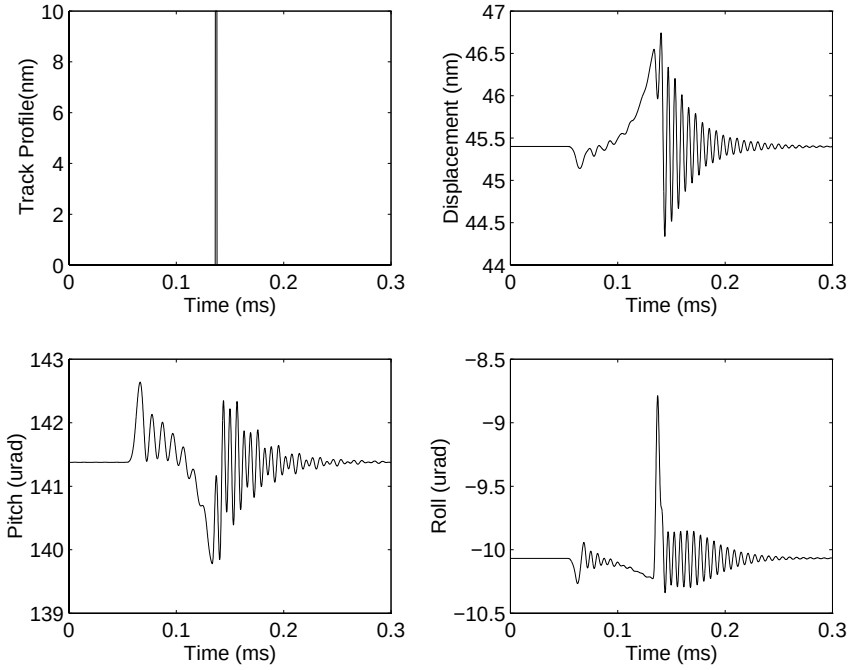

Figure 15: Responses of the 30% U slider to a 10 nm bump

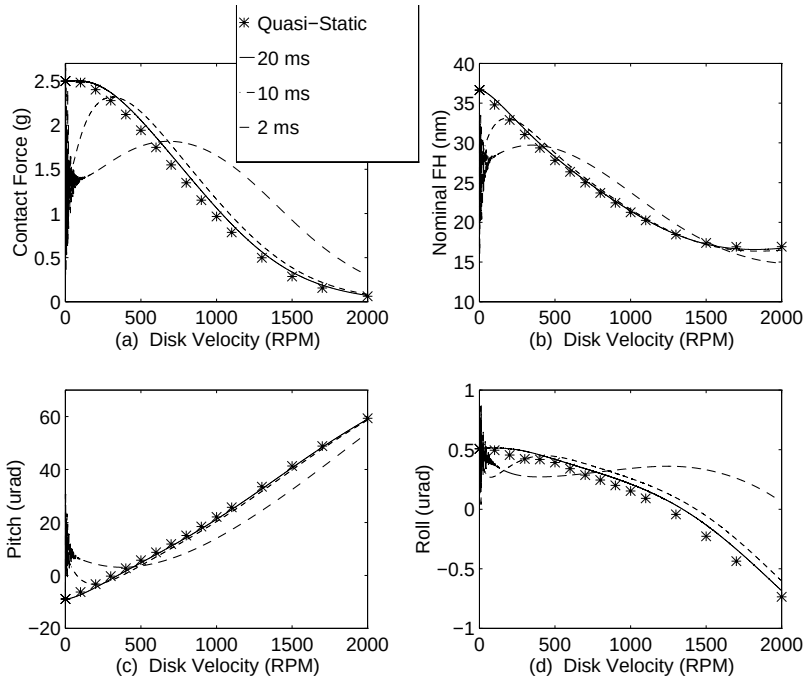

Figure 16: Effect of disk spin-up time

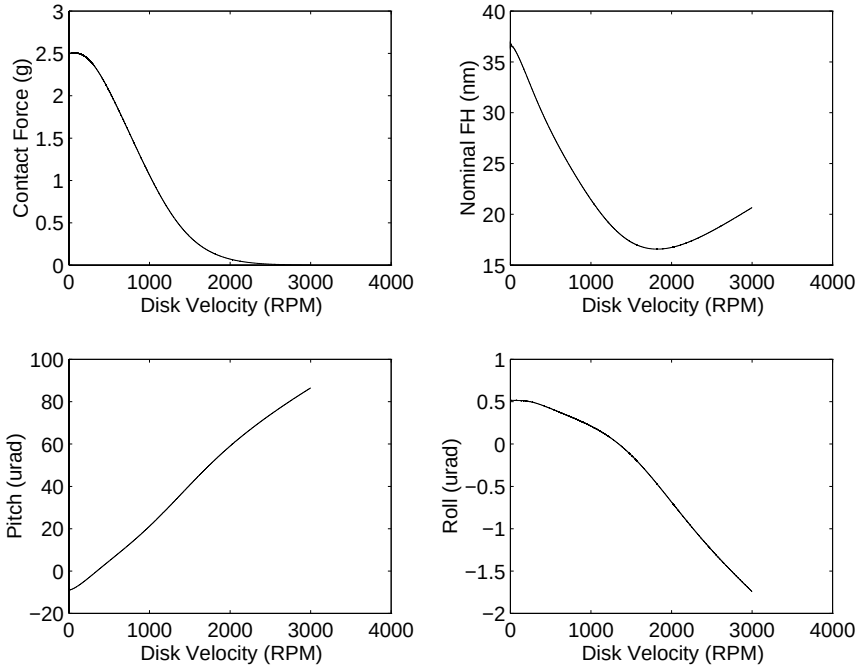

Figure 17: Contact takeoff results for TNPS slider

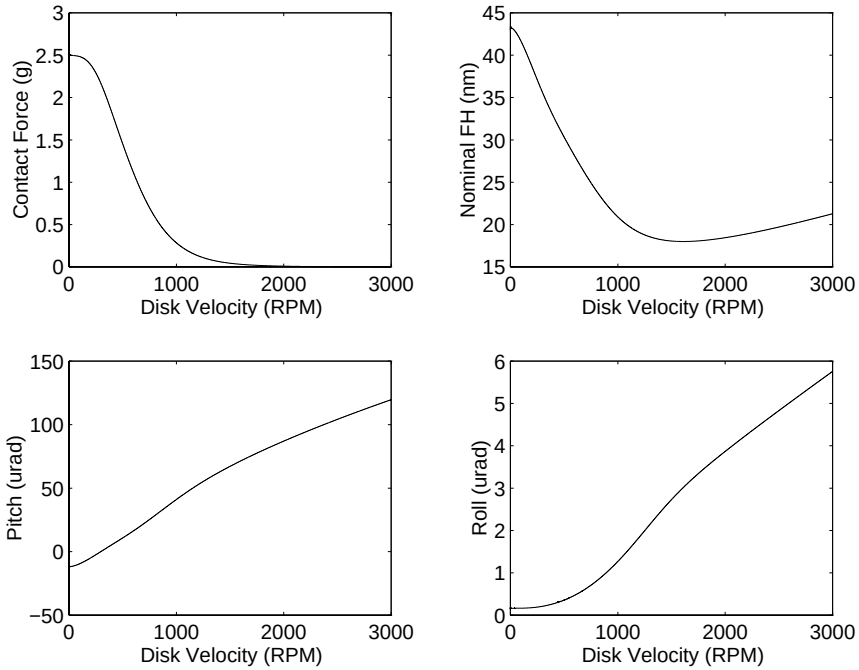

Figure 18: Contact takeoff results for Tri-K slider

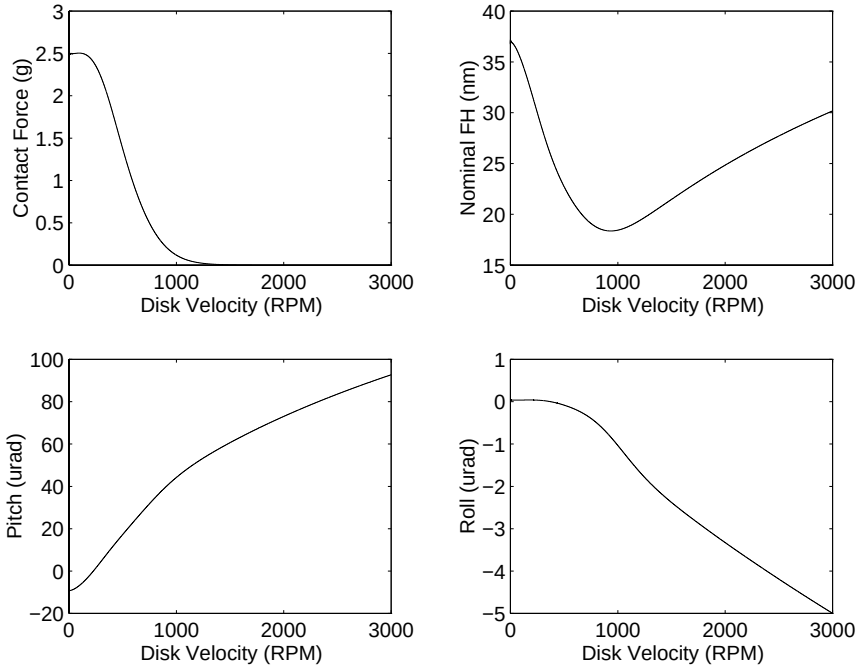

Figure 19: Contact takeoff results for U slider

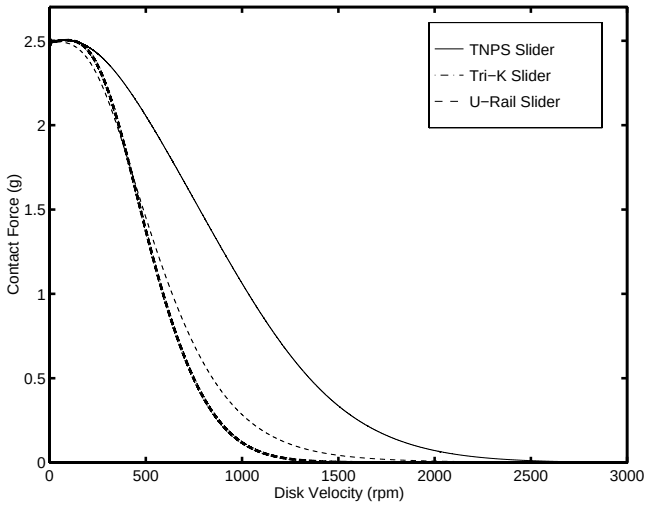

(a) Contact Force

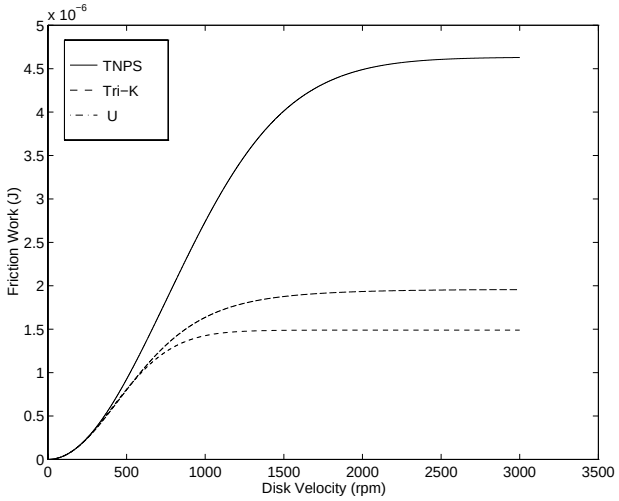

(b) Friction Work

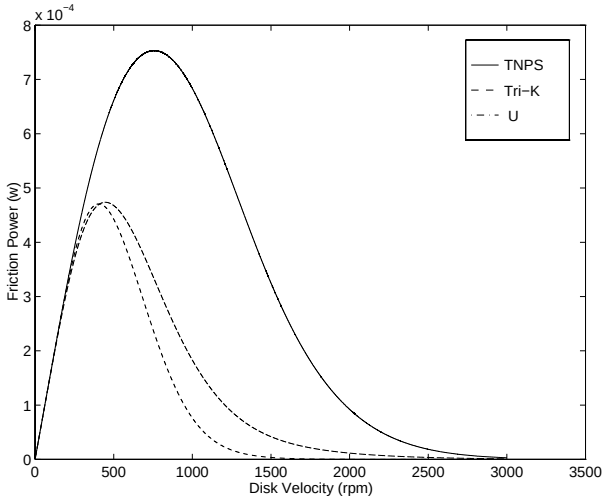

(c) Friction Power

Figure 20: Comparison of contact takeoff behavior

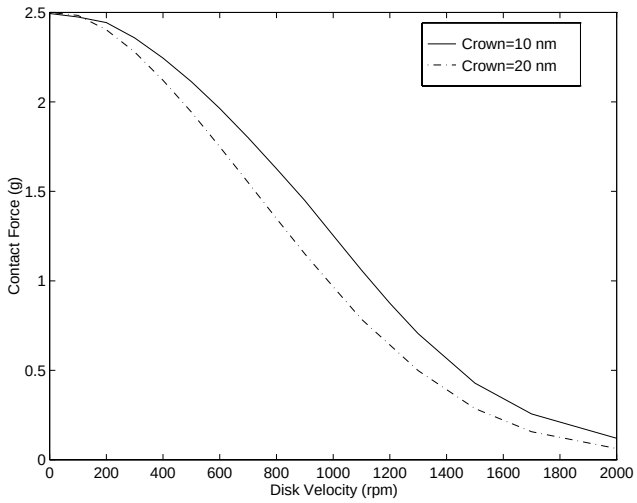

(a) Contact Force

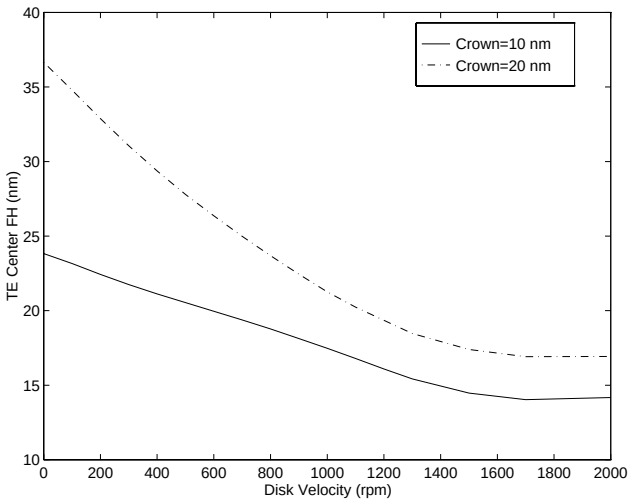

(b) TE Nominal FH

Figure 21: Crown effect on TOV and contact force for the TNPS slider

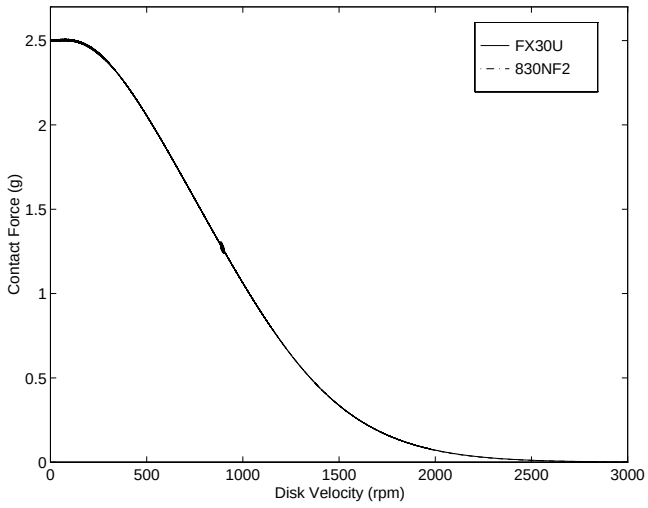

(a) Contact Force

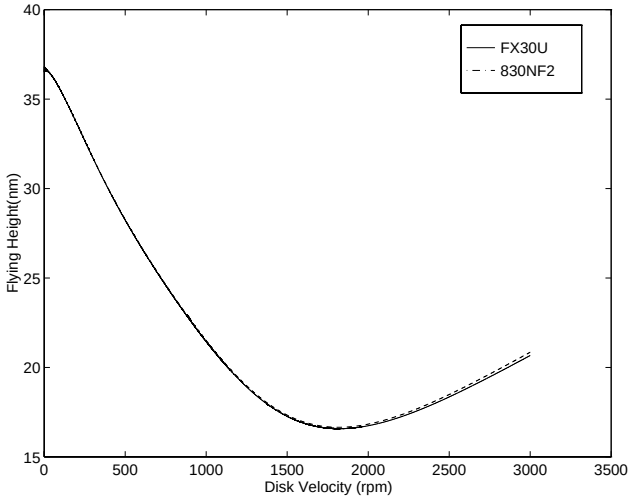

(b) CTE Nominal FH

Figure 22: Effect of suspension type

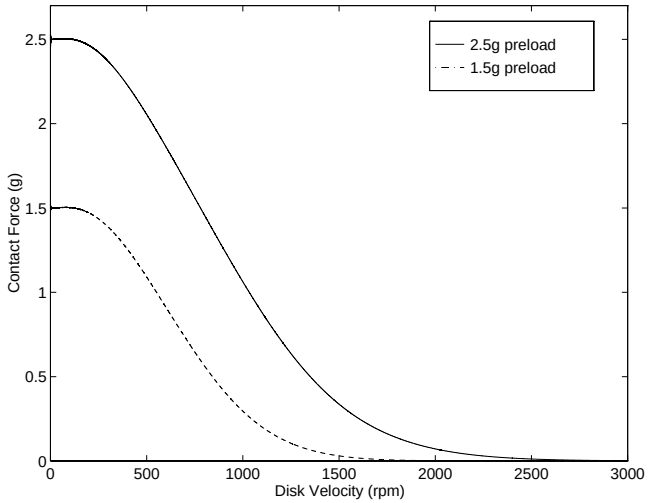

(a) Contact Force

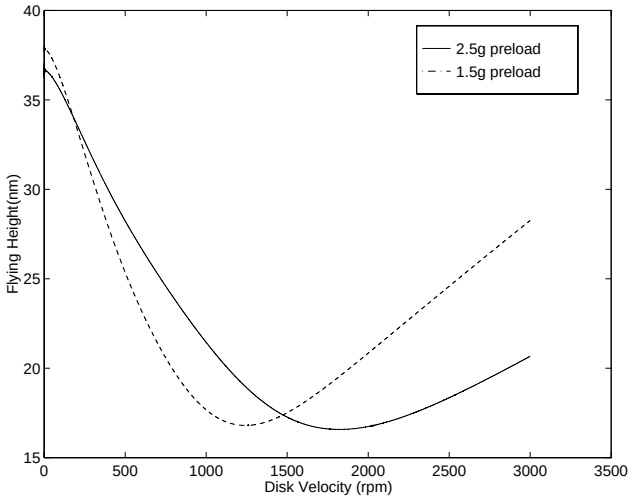

(b) CTE Nominal FH

Figure 23: Effect of suspension preload

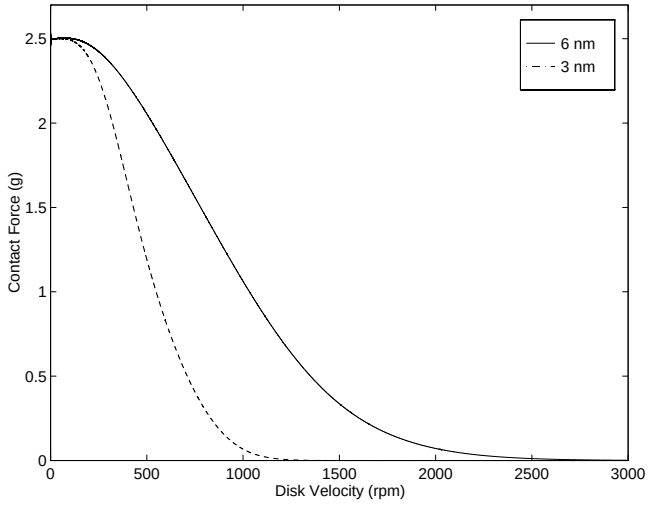

(a) Contact Force

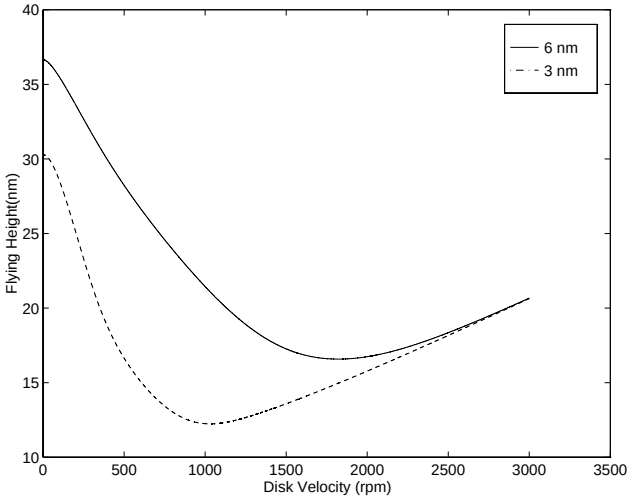

(b) CTE Nominal FH

Figure 24: Effect of the standard deviation of asperity heights

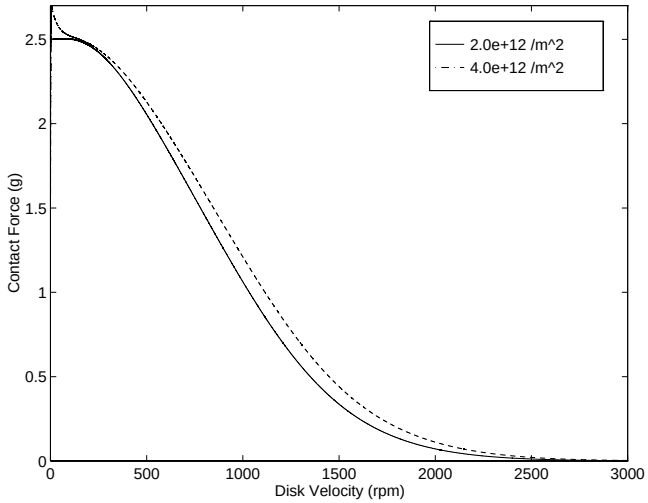

(a) Contact Force

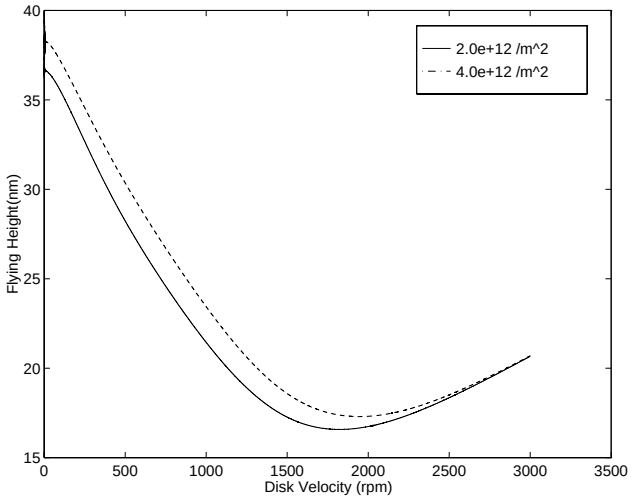

(b) CTE Nominal FH

Figure 25: Effect of asperity density

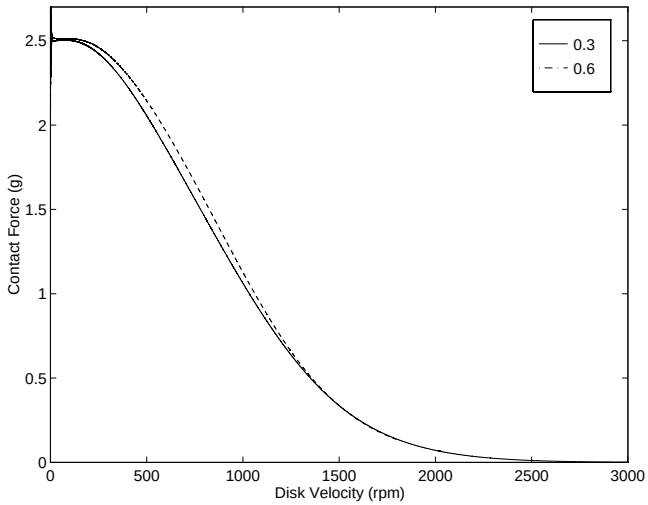

(a) Contact Force

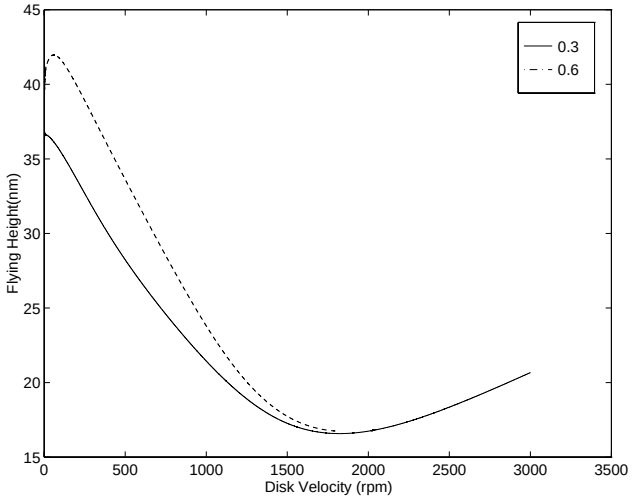

(b) CTE Nominal FH

Figure 26: Effect of dynamic friction coefficient